Journal of Catalysis 344 (2016) 817–830

Contents lists available at ScienceDirect

Journal of Catalysis

journal homepage: www.elsevier.com/locate/jcat

Acid strength and metal-acid proximity effects on methylcyclohexane ring contraction turnover rates and selectivities

William Knaeble, Enrique Iglesia [*]

Department of Chemical and Biomolecular Engineering, University of California, Berkeley, CA 94720, United States

ARTICLE INFO

Article history:
Received 27 May 2016
Revised 26 July 2016
Accepted 11 August 2016
Available online 17 September 2016

Keywords:
Keggin heteropolyacids
Methylcyclohexane ring-contraction
Bifunctional catalysis
Site proximity
Acid strength
Deprotonation energy
Diffusional enhancements of secondary reactions

ABSTRACT

Methylcyclohexane ring contraction is used here to assess the effects of acid strength and metal-acid site proximity on turnover rates and selectivities for bifunctional catalysts consisting of Keggin type polyoxometalates (POM) with different central atoms that act as Brønsted acids. Bifunctional catalysts with metal sites that fully equilibrate cycloalkanes and cycloalkenes give methylcyclohexene conversion rate constants that decreased exponentially with increasing deprotonation energy, a rigorous descriptor of acid strength, consistent with the ion-pair character of transition states that mediate the kinetically-relevant ring contraction of bound methylcyclohexoxide intermediates. The measured rates of formation of each alkylcyclopentane isomer, however, do not reflect their intrinsic formation kinetics, because of fast diffusion-enhanced interconversions within acid domains; thus, isomer selectivities cannot be used to infer, even indirectly, the strength of acid sites, as often proposed in previous studies. Selectivities reflect instead diffusional effects that become more severe as the number and strength of acid sites and the size and diffusive resistances increase within these acid domains, which shift, in turn, the products formed from relative abundances dictated by kinetics to those prescribed by thermodynamics. A rigorous accounting of these diffusional effects using a kinetic-transport model leads to ratios of intrinsic rate constants for the formation of the different alkylcyclopentane isomers that do not depend on acid strength, because all isomerization routes are mediated by bicyclo[3.1.0]hexyl cation transition states similar in the amount and location of charge and that therefore benefit to the same extent from the more stable conjugate anions characteristic of stronger acids.

1. Introduction

The contraction of methylcyclohexane rings to form alkylcyclopentanes on bifunctional catalysts consisting of Brønsted acid and metal functions is often used as a probe of acid strength and of the effects of confinement within amorphous and crystalline solid acids [1–4], and it is also of industrial importance because such chemistry is paramount for the effective conversion of ethylbenzene to xylene isomers [5,6]. Yet, connections between reactivity, selectivity, and acid strength remain empirical because of the challenges inherent in assessing the number and strength of acid sites and their consequential distances from the metal function, and the identity and reversibility of the elementary steps that mediate such reactions. These hurdles are overcome here by using Brønsted acids with known structure and acid strength, measuring acid site densities during catalysis, dispersing a metal function that maintains cycloalkane-cycloalkene equilibria, and rigorous mechanistic interpretation of measured rates and selectivities.

Tungsten polyoxometalate (POM) clusters with Keggin structures and charge-balancing protons ($H_{8-n}X^{n+}W_{12}O_{40}$) are Brønsted acids with uniform and well-defined atomic connectivity and diverse chemical composition ($X^{n+} = P^{5+}, Si^{4+}, Al^{3+}, Co^{2+}$) [7]. Their acid strength and the reactivity of their protons depend on their central atoms, because of their concomitant effects on the number of protons and on the stability of the conjugate anion [8]. Deprotonation energies (DPE) reflect the energy required for heterolytic cleavage of a proton from the conjugate base, thus providing a rigorous measure of acid strength accessible to calculation by density functional theory (DFT) for solids with known structures, such as Keggin POM clusters (1087–1143 kJ mol^{-1} for $H_{8-n}X^{n+}W_{12}O_{40}$; X = P, Si, Al, or Co in order of increasing DPE) [8,9].

Our recent studies have shown that first-order rate constants for the isomerization of acyclic alkenes [10] and for the dehydration of alkanols [7,11,12] (per accessible H^+) decrease exponentially with increasing DPE (decreasing acid strength) for Keggin POM clusters with different central atoms (P, Si, Al, Co); such

---

[*] Corresponding author. Fax: +1 510 642 4778.
E-mail address: iglesia@berkeley.edu (E. Iglesia).

http://dx.doi.org/10.1016/j.jcat.2016.08.007
0021-9517/

trends reflect the stability of ion-pair transition states (TS), which benefits from more stable conjugate anions. The sensitivity of alkene isomerization rate constants to DPE is similar for different hexene isomer reactants [10], because the amount and location of the positive charge are similar among the transition states that mediate such reactions. Consequently, alkene isomerization selectivities are insensitive to acid strength, because they solely reflect the stability of the protonated gaseous analogs of each isomerization of TS. The isomerization selectivities observed, however, do not only reflect such intrinsic selectivities, because of the ubiquitous role of fast secondary alkene interconversions that occur locally within porous acid domains before alkenes convert to alkanes either via hydrogen transfer at acid sites or via reactions with H_2 at metal sites in bifunctional catalysts [10].

Here, ring contraction rate constants (per H^+) for methylcyclohexane ring contraction are examined through mechanistic interpretations of rate and selectivity data combined with titrations of accessible protons during catalysis. Measured selectivities differ from their intrinsic values because of diffusion-enhanced interconversions among alkylcyclopentene products within acid domains. Such diffusional enhancements are stronger on catalysts with stronger and/or more abundant acid sites and in acid domains of larger size or smaller diffusion coefficients. Furthermore, experimental results indicate that rate constants for the formation of each primary alkylcyclopentane isomer increase exponentially with decreasing DPE values to the same extent, leading to intrinsic selectivities that do not depend on acid strength. These data show, once again, that ion-pair transition states of similar charge are affected similarly by the stability of the conjugate anion. Thus, measured selectivities (even at differential conversions) cannot be taken as evidence for acid strength [1,2,13,14]; the preferential formation of the products formed in more demanding isomerization routes does not reflect a concomitant preference for such reactions on stronger acids or in microporous acids. Instead, such trends arise from intrapellet gradients of product alkenes that become more severe on more reactive protons (stronger acids) or within porous media in which molecules diffuse more slowly or over greater distances. In the most severe cases, diffusion-enhanced interconversions move selectivities away from those determined by the relative rates at which primary isomer products are formed and toward their thermodynamic values.

2. Experimental methods

2.1. Catalyst preparation

Detailed catalyst synthesis procedures have been reported elsewhere [10]. $H_3PW_{12}O_{40}$ (Sigma-Aldrich; Reagent Grade; CAS #12501-23-4), $H_4SiW_{12}O_{40}$ (Aldrich; >99.9%; CAS #12027-43-9), $H_5AlW_{12}O_{40}$ (prepared according to [15]), and $H_6CoW_{12}O_{40}$ (prepared according to [16,17]) were supported on amorphous SiO_2 (Cab-O-Sil HS-5; 310 $m^2\ g^{-1}$; 1.5 $cm^3\ g^{-1}$ pore volume) at loadings of 0.04 and 0.20 POM $(nm^2\text{-}SiO_2)^{-1}$ using incipient wetness impregnation methods. SiO_2-supported POM clusters will be denoted herein as "H_nXW/SiO_2", where n is the proton stoichiometry. ^{31}P-MAS-NMR spectra showed that their dispersion onto the SiO_2 support and their use in catalysis retained the essential features of the NMR spectra of intact $H_3PW_{12}O_{40}$ Keggin structures [10]. Transmission electron micrographs showed that POM clusters are present as isolated clusters with a minority of two-dimensional aggregates at these POM surface densities (0.033–0.067 POM $(nm^2\text{-}SiO_2)^{-1}$) [10].

Pt/Al_2O_3 (1.5 wt% Pt) was prepared by incipient wetness impregnation of treated $\gamma\text{-}Al_2O_3$ (Sasol SBa-200; 193 $m^2\ g^{-1}$, 0.57 $cm^3\ g^{-1}$ pore volume; treated in dry air (UHP Praxair; 0.5 $cm^3\ g^{-1}\ s^{-1}$) at 923 K for 18 ks) with aqueous H_2PtCl_6 solutions (Aldrich; CAS #16941-12-1) [10]. The Pt dispersion (90%) was determined by H_2 chemisorption at 313 K (Quantasorb analyzer; Quantachrome Corp.) using a 1:1 H:Pt stoichiometry [10]. Pt/Al_2O_3 and H_nXW/SiO_2 (X = P, Si, Al, or Co) catalysts were mixed as intimate aggregates (<20 μm) using a mortar and pestle; these fine powders were pressed into wafers and then crushed and sieved to retain 125–180 μm aggregates. The composition of these mixtures is reported as the ratio of surface Pt-atoms (from H_2 chemisorption) to H^+ in POM clusters (from titrations with 2,6-di-*tert*-butylpyridine during catalysis; Section 2.2).

2.2. Ring contraction rate measurements and titrations of protons with 2,6-di-tert-butylpyridine during catalysis

Reaction rates and selectivities were measured on samples (0.040–0.103 g) packed within a stainless steel tubular reactor (3/8 in. O.D.) with plug-flow hydrodynamics. Reactor temperatures were measured with two K-type thermocouples (Omega; ±0.2 K), one held against the external reactor wall and the other held within a 1/16 in. stainless steel sheath aligned axially along the bed; temperatures were controlled using a resistively-heated furnace and PID control strategies (Watlow Series 982 controller). Transfer lines were kept at 423 K to prevent condensation of reactants, products, and titrants. A backpressure regulator was used to control pressure (Equilibar, model EB1LF2). Physical mixtures of Pt/Al_2O_3 and H_nXW/SiO_2 were treated in flowing H_2 (Praxair UHP) at 2 bar (0.16 $cm^3\ s^{-1}$ at STP) by heating to 473 K at 0.083 $K\ s^{-1}$ and holding for 4 ks before catalytic measurements. Liquid methylcyclohexane (MCH; Sigma-Aldrich; >99%) was used without further purification and vaporized at 523 K into a flowing H_2 (UHP Praxair) stream using a liquid syringe pump (Cole-Palmer 74900 Series). Molar MCH and H_2 flow rates were set using electronic mass flow controllers to maintain a given (MCH/H_2) molar ratio and low MCH conversions (<10%).

Reactants and products in the reactor effluent were separated chromatographically (HP-1 column; 0.32 mm ID × 50 m, 1.05 μm film; Agilent) and detected using flame ionization (Agilent 6890 N GC). The predominant products detected were as follows: ethylcyclopentane (ECP), *cis*-1,3-dimethylcyclopentane (c13DMCP), *trans*-1,3-dimethylcyclopentane (t13DMCP), *trans*-1,2-dimethylcyclopentane (t12DMCP), 1,1-dimethylcyclopentane (11DMCP), several acyclic heptane isomers, and methylcyclopentane. *cis*-1,2-Dimethylcyclopentane (c12DMCP) and MCH did not elute separately from the column; therefore, c12DMCP formation rates were calculated from its equilibrium constant with t12DMCP at 473 K [18]. 13DMCP chemical isomers (c13DMCP and t13DMCP) were detected at a nearly constant ratio ([c13DMCP]/[t13DMCP] = 1.071 ± 0.008), leading us to assume similar equilibration for cis and trans 12DMCP. The c12DMCP and t12DMCP isomers (and the c13DMCP and t13DMCP isomers) are treated as a 12DMCP (and 13DMCP) lumped products. The concentration of any product (t12DMCP, c12DMCP, and ECP) present as trace impurities (<0.0013 mol%) in MCH reactants was subtracted from those detected in the effluent in determining product formation rates. The rates of formation of each product were also corrected for their approach to equilibrium for the reactions that form them from MCH using the following:

$$r_{forward} = r_{net}\left(1 - \left(\frac{P_P}{P_{mch}}\right)\frac{1}{K_{mch,P}}\right)^{-1} \quad (1)$$

in which (P_P/P_{mch}) is the ratio of product and MCH pressures in the effluent and $K_{mch,P}$ is their equilibrium constant at 473 K, derived from reported thermodynamic data [18,19]. Catalyst deactivation (half-lives between 14 and 72 ks) was observed on all catalysts during kinetic experiments. Rates measured periodically at a standard condition (4 kPa MCH and 235 kPa H_2) were used to correct all rate data for any intervening deactivation.

Titrations during catalysis were performed by dissolving 2,6-di-*tert*-butylpyridine (DTBP, Aldrich; >97%; CAS #585-48-8) in liquid MCH reactants (between 7.7×10^{-6} and 1.1×10^{-3} mol%) and vaporizing this mixture into flowing H_2 stream (UHP Praxair) at 523 K to give DTBP pressures between 0.03 and 4.4 Pa. Ring contraction rates and DTBP uptakes were determined using the chromatographic protocols described above. The number of DTBP titrants required to suppress MCH conversion rates reflects the number of H^+ present in POM/SiO_2 samples during catalysis [20]. The complete suppression of reaction rates would confirm that these isomerization reactions occur exclusively on Brønsted acid sites without detectable contributions from any Lewis acid sites present in the samples.

Symbols and notations used herein are summarized in Appendix A following the main text.

3. Results and discussion

3.1. Elementary steps, rates, and product selectivities for methylcyclohexane ring contraction

Methylcyclohexane (MCH) ring contraction rates and selectivities were measured on silica-supported POM clusters (H_nXW/SiO_2) with different central atoms (X = P, Si, Al, and Co) present as bifunctional physical mixtures with Pt/Al_2O_3. MCH ring contraction reactions predominately formed ECP, 12DMCP, and 13DMCP at all conditions and on all catalysts (>98% carbon selectivity), with only trace amounts of 11DMCP isomers observed (<1% carbon selectivity at short residence times). Ring contraction rates (per mass of catalyst) were much higher on bifunctional mixtures containing H_nXW/SiO_2 than on monofunctional Pt/Al_2O_3 or H_nXW/SiO_2 catalysts (by factors >100), indicating that ring contraction occurs on acid sites but requires the intervening formation of methylcyclohexene isomers on the metal function, consistent with previous results for the isomerization of other saturated hydrocarbons [10,21,22].

Titration with 2,6-di-*tert*-butylpyridine (DTBP) during reaction gave rates that decreased monotonically with increasing DTBP uptakes on all catalysts; these rates ultimately reached undetectable levels after all protons were titrated and uptakes reached constant values (shown for H_4SiW/SiO_2 in Fig. SI-1; supporting information (SI)). Thus, MCH ring contraction occurs only on Brønsted acid sites, and DTBP titrates all protons in H_nXW/SiO_2 co-catalysts. Ring contraction turnover rates are reported here on the basis of the number of H^+ titrated by DTBP in each sample (Table 1).

MCH ring contraction rates on bifunctional mixtures containing H_nXW/SiO_2 and Pt/Al_2O_3 are limited by the ring isomerization of methylcyclohexenes ($MCH^=$) on Brønsted acid sites when hydrogenation-dehydrogenation equilibrium [23] is maintained by the metal function at the external boundaries of the acid domains (defined as proton-containing regions devoid of metal sites), and $MCH^=$ consumption rates are slow enough to preclude $MCH^=$ concentration gradients within these acid domains. Catalyst deactivation during MCH ring isomerization kinetic experiments prevented direct comparisons of experimental data among bifunctional mixtures with different initial H^+ densities within acid domains and (Pt_S/H^+) ratios, the unequivocal confirmation of kinetic control [24]. First-order rate constants for $MCH^=$ ring contraction (per H^+), however, were more than ten-fold smaller than those for 2-methylpentene isomerization (per H+) on these same catalysts ([10]). The latter values did not depend on either (Pt_S/H^+) ratios ((Pt_S/H^+) = 6.2–22.9 for H_3PW/SiO_2-Pt/Al_2O_3 mixtures) or H^+ densities (0.006 and 0.070 H^+ $(nm^3\text{-}SiO_2)^{-1}$ for H_3PW/SiO_2-Pt/Al_2O_3 mixtures), thus establishing the kinetic origins of those measured rate constants. Therefore, the initial (Pt_S/H^+) ratio ($(Pt_S/H^+)_0$ = 5.4) and proton density (0.022 H^+ $(nm^3\text{-}SiO_2)^{-1}$) for the H_3PW/SiO_2-Pt/Al_2O_3 mixture, and those for the mixtures containing the other POM acids (<0.022 H^+ $(nm^3\text{-}SiO_2)^{-1}$ and $(Pt_S/H^+)_0$ > 1.7), which have lower MCH ring contraction turnover rates (per H^+) than H_3PW (Fig. 1), are considered to be sufficient to maintain alkane-alkene dehydrogenation-hydrogenation equilibrium during MCH reactions outside acid domains and to avoid corruptions of measured ring contraction turnover rates by transport restrictions.

Fig. 1 shows MCH ring contraction turnover rates (per H^+) as a function of (MCH/H_2) inlet molar ratios on H_nXW/SiO_2-Pt/Al_2O_3 mixtures with P, Si, Al, and Co central atoms ((Pt_s/H^+) = 1.7–38). MCH ring contraction turnover rates increased with increasing (MCH/H_2) ratios, linearly at first and then more gradually at higher reactant ratios; these rates did not depend on H_2 pressures (191–442 kPa H_2) for each given (MCH/H_2) ratio on any of the H_nXW/SiO_2-Pt/Al_2O_3 mixtures (Fig. 1). These data are consistent with the full equilibration of methylcyclohexane and all methylcyclohexene isomers on Pt sites and with ring contraction rates that depend only on the concentration of these $MCH^=$ species, as shown next by the interpretation of measured rates in terms of a sequence of plausible ring contraction elementary steps.

Scheme 1 shows a sequence of elementary steps and the overall MCH ring contraction stoichiometric reactions on metal-acid mixtures at conditions of MCH-H_2-$MCH^=$ equilibration on the Pt function for all methylcyclohexene regioisomers (Scheme 1, Step 1 shown for the case of 1-methylcyclohexene reactant isomers); at these conditions, $MCH^=$ concentrations depend only on (MCH/H_2) ratios and their respective equilibrium constants ($K_{d,mch}$). Methylcyclohexenes diffuse into acid domains (Scheme 1, Step 2) where they equilibrate with H^+ to form the corresponding alkoxides in quasi-equilibrated steps (Scheme 1, Step 3). Methylcyclohexoxides with different attachment points equilibrate via rapid hydride shifts in alkoxides [21,25]. These alkoxides then isomerize to ethylcyclopentoxides or dimethylcyclopentoxides via ring contraction elementary steps (Scheme 1). Steps 4a-c illustrates the specific formation of the ethylcyclopent-2-oxide, 1,2-dimethylcyclopent-3-oxide, and 1,3-dimethylcyclopent-2-oxide isomers.

We propose here, based on DFT treatments [26], that these steps are mediated by ion-pair transition states containing

Table 1
Number of accessible H^+ per POM clusters measured by chemical titration of protons with 2,6-di-*tert*-butylpyridine[a] during methylcyclohexane isomerization[b] on H_nXW/SiO_2-Pt/Al_2O_3 (X = P, Si, Al, Co) mixtures.

Catalyst	POM content (wt%)	POM areal density (POM $(nm^2\text{-}SiO_2)^{-1}$)	Accessible H^+ (per POM)	H^+ Volumetric density (H^+ $(nm^3\text{-}SiO_2)^{-1}$)	Pt_s/H^+ ratio
$H_3PW_{12}O_{40}$	10	0.067	1.6	0.022	5.4
$H_4SiW_{12}O_{40}$	5	0.034	2.6	0.018	3.3
$H_5AlW_{12}O_{40}$	5	0.033	2.5	0.020	1.7
$H_6CoW_{12}O_{40}$	5	0.039	0.22	0.002	38

[a] Assuming a 1:1 DTBP:H^+ adsorption stoichiometry.

[b] 4 kPa methylcyclohexane, 218 kPa H_2, 473 K.

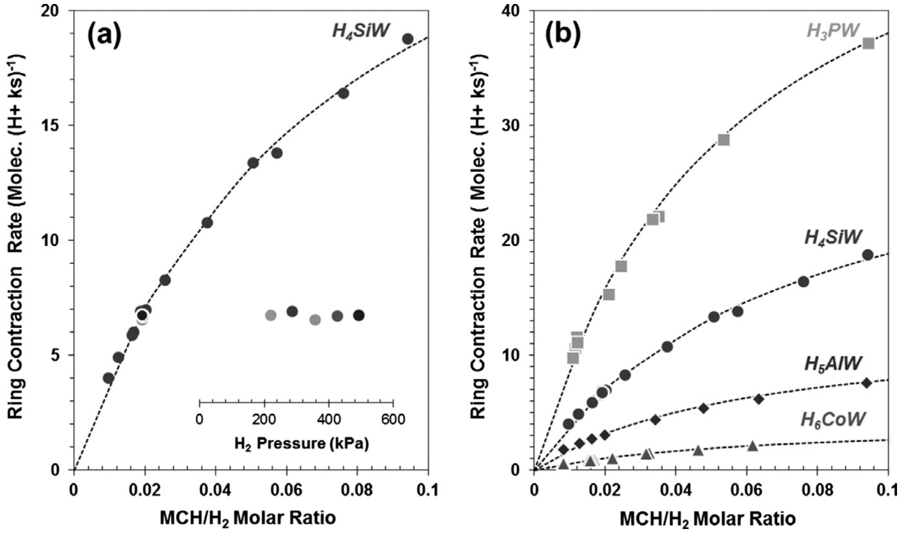

Fig. 1. (a) Methylcyclohexane ring contraction turnover rate as functions of the (MCH/H_2) ratio and H_2 pressure (shown at the inset for a MCH/H_2 ratio of 0.02) on a H_4SiW/SiO_2 mixture with Pt/Al_2O_3 ($Pt_S/H^+ = 3.3$, 0.018 H^+ (nm^3-SiO_2)$^{-1}$) and (b) as functions of the (MCH/H_2) ratio on Pt/Al_2O_3 mixtures with H_3PW/SiO_2 ($Pt_S/H^+ = 5.4$, 0.022 H^+ (nm^3-SiO_2)$^{-1}$; ■), H_4SiW/SiO_2 ($Pt_S/H^+ = 3.3$, 0.018 H^+ (nm^3-SiO_2)$^{-1}$; ●), H_5AlW/SiO_2 ($Pt_S/H^+ = 1.7$, 0.020 H^+ (nm^3-SiO_2)$^{-1}$; ◆), and H_6CoW/SiO_2 ($Pt_S/H^+ = 38$, 0.002 H^+ (nm^3-SiO_2)$^{-1}$; ▲) (reaction conditions: 473 K, 191–442 kPa H_2). Dashed lines represent the regression of the data to the functional form of Eq. (2).

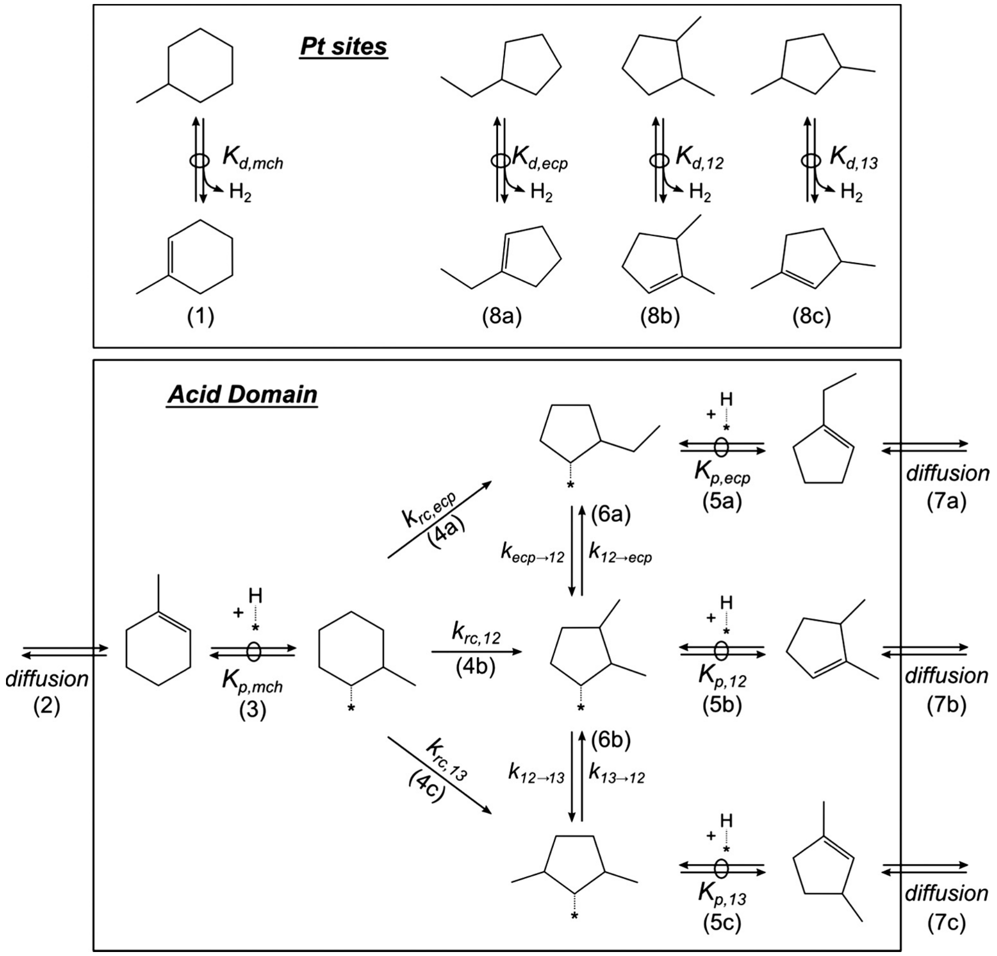

Scheme 1. Elementary steps and chemical reactions involved in methylcyclohexane ring contraction on metal-acid mixtures that establish methylcyclohexane/methylcyclohexene equilibrium. Chemical reactions are shown for the (de)hydrogenation on metal sites (Pt/Al_2O_3) and elementary steps for acid-catalyzed routes on H_nXW/SiO_2 (X = P, Si, Al, Co). Bonds to the Brønsted active site are denoted as "$*$" in molecular structures.

corner-protonated bicyclo[3.1.0]hexyl cations, in which C—C bonds cleave and form in concerted steps, consistent with TS structures previously proposed by others for ring contractions of gaseous cyclohexyl [27,28], methylcyclohexyl [29], and 1,2-dimethylcyclohexylium [30] cations and of cyclohexene catalyzed by zeolitic acids [31]. Cyclopentoxide products deprotonate via β-hydrogen transfer to POM oxygen atoms in quasi-equilibrated steps to form the respective gaseous alkylcyclopentene isomers (Scheme 1, Steps 5a-c shown for ethylcyclopent-1-ene, 1,2-dimethylcyclopent-2-ene, and 1,3-dimethylcyclopent-1-ene isomers, respectively); these isomers can readsorb on H^+ sites as they diffuse through acid domains to re-form alkoxides that can, in turn, undergo secondary isomerizations to form other alkylcyclopentoxides and alkyl cyclopentenes. Step 6a (Scheme 1) illustrates these reactions for ethylcyclohex-2-oxide and 1,2-dimethylcyclopent-3-oxide interconversions and Step 6b shows the steps for 1,2-dimethylcyclopent-3-oxide and 1,3-dimethylcyclopent-2-oxide interconversions. Gaseous alkylcyclopentene isomers that exit an acid domain (Scheme 1, Step 7a-c shown for ethylcyclopent-1-ene, 1,2-dimethylcyclopent-2-ene, and 1,3-dimethylcyclopent-1-ene, respectively) rapidly hydrogenate on Pt sites and equilibrate with their respective cycloalkane isomers (Scheme 1, Step 8a-c for ECP, 12DMCP, and 13DMCP formation, respectively). Alkene (and alkoxide) regioisomers with the same carbon backbone are treated here as lumped chemical pseudo-species because of their equilibrated interconversions [26]. The lumped cycloalkenes with a given backbone are denoted here by a superscript “ = ” and their respective alkoxides by “⁎”, in both cases without specifying the location of the surface attachment or of the C═C bond (e.g., MCH, $MCH^=$, and MCH^* for methylcyclohexane, methylcyclohexene isomers, and methylcyclohexoxide isomers; see Nomenclature).

Pseudo-steady-state concentrations of alkoxides and quasi-equilibration between $MCH^=$ isomers and their MCH^* counterparts, taken together with Langmuir adsorption kinetics and MCH^* and H^+ as the most abundant surface intermediates (MASI), give an equation for MCH ring contraction rates to form all alkylcyclopentene isomers:

$$\frac{r_{rc}}{[H^+]} = \frac{k_{rc}K_{p,mch}K_{d,mch}\left(\frac{[MCH]}{[H_2]}\right)}{1 + K_{p,mch}K_{d,mch}\left(\frac{[MCH]}{[H_2]}\right)} \tag{2}$$

where

$$k_{rc} = k_{rc,ecp} + k_{rc,12} + k_{rc,13} \tag{3}$$

represents the sum of rate constants for MCH^* ring contraction to form each skeletal isomer (each consisting of isomers with equilibrium double-bond locations and cis-trans configurations). Here, $[H^+]$ is the total number of protons, $K_{p,mch}$ is the equilibrium constant for MCH^* formation from $MCH^=$ (illustrated for methylcyclohex-1-oxide in Scheme 1), and $k_{rc,P}$ is the rate constant for MCH^* ring contraction to form a given product ($k_{rc,ecp}$, $k_{rc,12}$, and $k_{rc,13}$ for $ECP^=$, $12DMCP^=$, and $13DMCP^=$ formation, respectively). The first two terms in the denominator reflect the relative coverages of MCH^* and unoccupied H^+; the terms corresponding to bound alkylcyclopentoxides are much smaller at the low prevalent concentration of gaseous products. The dashed curves in Fig. 1 represent the regression of these rate data to the functional form of Eq. (2) with the reported thermodynamics for MCH-$MCH^=$ equilibration ($K_{d,mch}$ = 5.0 Pa at 473 K referenced to the lumped chemical pseudo-species, $MCH^=$ [32–35]); the regressed k_{rc} and $K_{p,mch}$ values and their product are shown in Table 2 for all H_nXW/SiO_2 acids. These parameters accurately describe all rate data, as shown by their small uncertainty intervals (Table 2) and the dashed lines in Fig. 1.

Table 2
Methylcyclohexane ring contraction rate constants ($k_{rc}K_{p,mch}$ and k_{rc}) and protonation equilibrium constants ($K_{p,mch}$) measured on $H_nXW_{12}O_{40}/SiO_2$-Pt/Al_2O_3 (X = P, Si, Al, Co) mixtures (473 K).

Catalyst	$k_{rc}K_{p,mch}$ [a,d]	k_{rc} [b,d]	$K_{p,mch}$ [c,d]
$H_3PW_{12}O_{40}$	216 ± 3	59 ± 3	3.7 ± 0.2
$H_4SiW_{12}O_{40}$	88 ± 1	33 ± 1	2.7 ± 0.1
$H_5AlW_{12}O_{40}$	42 ± 2	12 ± 1	3.4 ± 0.4
$H_6CoW_{12}O_{40}$	13.9 ± 0.3	4.3 ± 0.3	3.3 ± 0.3

[a] molec. $(H^+\ ks\ Pa)^{-1}$.
[b] molec. $(H^+\ ks)^{-1}$.
[c] Pa^{-1}.
[d] Errors represent the 95% confidence intervals of the parameters in the linearized form Eq. (2) obtained from the method of least-squares.

Product selectivities are defined here as the formation rate of a given product “P” ($r_{rc,P}$) divided by the combined rate of MCH conversion to all products (r_{rc}):

$$S_{m,P} = \frac{r_{rc,p}}{r_{rc}} \tag{4}$$

(“P” = ecp, 12, or 13 for ECP, 12DMCP, and 13DMCP). Fig. 2 shows ECP, 13DMCP, and 12DMCP selectivities as a function of space velocity (defined as moles MCH $(ks\ [H^+])^{-1}$) for different H^+ densities (densities varied by allowing deactivation to occur) on H_4SiW/SiO_2-Pt/Al_2O_3 at differential MCH conversions (<2.1%). A decrease in H^+ density led to higher ECP selectivities and lower 12DMCP and 13DMCP selectivities, even though changes in conversion induced by varying space velocity (for a given H^+ density)

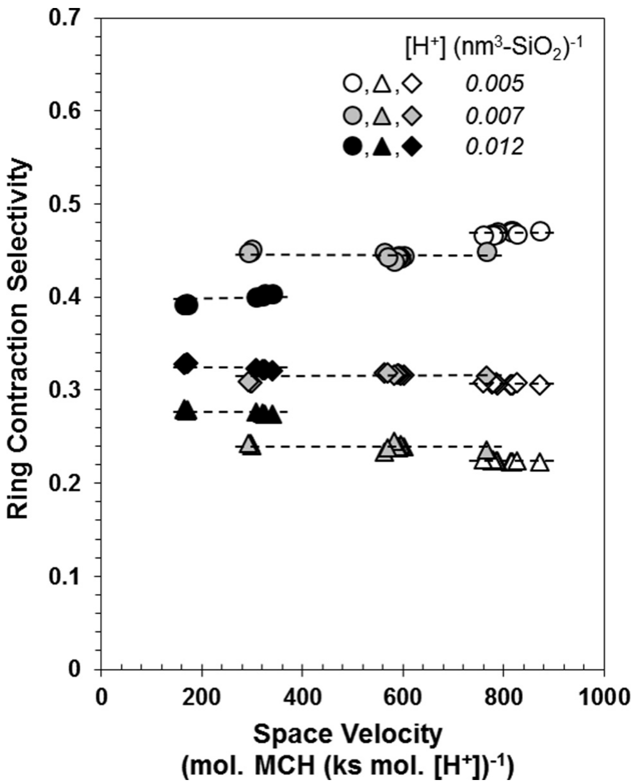

Fig. 2. Measured ethylcyclopentane (●), 1,3-dimethylcyclopentane (▲), and 1,2-dimethylcyclopentane (◆) selectivities as functions of space velocity for different H^+ densities (0.005, 0.007 and 0.012 $[H^+]$ $(nm^3\text{-}SiO_2)^{-1}$) on H_4SiW/SiO_2-Pt/Al_2O_3 ($Pt_S/[H^+]_0$ = 3.3) at differential MCH conversions (<2.1%), $[MCH]/[H_2]$ ratios below 0.026, total reactant flow rates between 3.5 and 7.0 mmol ks^{-1}, pressures between 220 and 500 kPa, and 473 K. The dashed lines are the average selectivity for each product at each acid domain H^+ density.

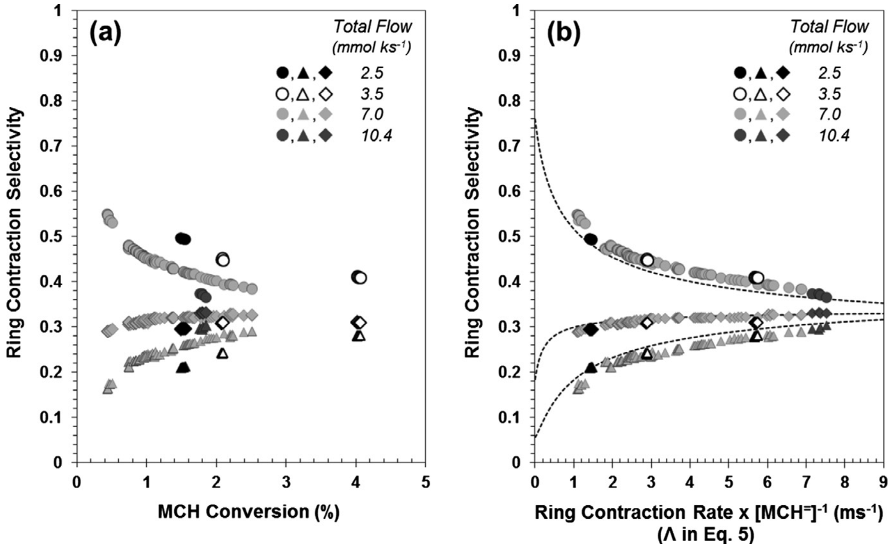

Fig. 3. Measured ethylcyclopentane (●), 1,3-dimethylcyclopentane (▲), and 1,2-dimethylcyclopentane (◆) selectivities as functions of (a) methylcyclohexane conversion and (b) measured ring contraction rate per volume of catalyst normalized to the molar concentration of $MCH^=$ (Λ in Eq. (5)) for different total reactant molar flow rates (2.5, 3.5, 7.0 and 10.4 mmol ks^{-1}) on H_4SiW/SiO_2-Pt/Al_2O_3 ($Pt_S/[H^+]_0$ = 3.3, 0.018 $[H^+]_0$ $(nm^3$-$SiO_2)^{-1}$) at several [MCH]/[H_2] ratios (0.01–0.10) and system pressures (220–500 kPa) at 473 K. The dashed lines in (b) are best fits of selectivity data measured on all catalysts (Fig. 4) to the functional form of Eq. (13).

did not influence selectivities. Fig. 3a shows ECP, 13DMCP, and 12DMCP selectivities as a function of MCH conversion at different reactant molar flow rates on H_4SiW/SiO_2-Pt/Al_2O_3. MCH conversions at each molar flow rate were smaller at longer times, because of more extensive deactivation, and at higher [MCH]/[H_2] molar ratios, because acid sites become preferentially covered by [MCH^*], thus inhibiting secondary interconversions. Such changes in MCH conversion (at each given total molar flow rate) increased ECP selectivity and decreased 12DMCP and 13DMCP selectivities; they resulted in selectivity curves that depended only on MCH conversion for each product at each total molar flow rate.

The strong effects of H^+ densities on selectivities, taken together with selectivity values that are insensitive to space velocities (Fig. 2), indicate that measured selectivities depend primarily on MCH conversion within each acid domain (a function of H^+ density and site coverage) and not, at a given H^+ density and $MCH^=$ pressure, on its overall conversion along the bed (a function of space velocity). Therefore, the observed differences in measured selectivities (at a given MCH conversion; Fig. 3a) for different reactant flow rates reflect different reaction times, which determine the number of remaining active sites, or the prevalent $MCH^=$ pressure, which set the fraction of these sites covered by MCH^* ($K_{p,mch}[MCH^=]$) and thus unavailable for the binding and isomerization of products. Clearly, differences in measured selectivities among catalysts that convert different fractions of MCH within each acid domain cannot be taken as evidence (even at a given MCH conversion) for the relative rates of formation of ring contraction product formed directly from $MCH^=$ as primary products.

The role of secondary reactions driven by concentration gradients of alkylcyclopentenes within acid domains makes ring contraction rates per volume of silica support divided by $MCH^=$ concentrations (calculated from the [MCH]/[H_2] ratio and $K_{d,mch}$):

$$\Lambda = \frac{r_{rc}}{V_{cat}[MCH^=]}, \tag{5}$$

instead of MCH conversion, the appropriate benchmark for comparing selectivities among catalysts, because the extent of these secondary interconversions depends on the reactivity and coverage of acid sites (like MCH conversion), but not on reactant flow rates (unlike MCH conversion). Fig. 3b depicts the same data as in Fig. 3a, but as a function of Λ instead of MCH conversion. All selectivity ratios become single-valued functions of Λ and unaffected by MCH conversion, [MCH]/[H_2] ratio, or MCH and H_2 pressures. These selectivities are also independent of the central atom in H_nXW/SiO_2-Pt/Al_2O_3 mixtures (P, Si, Al, and Co central atoms; (Pt_s/H^+) = 1.7–38) for a given Λ value (Fig. 4), despite the very different reactivities and acid strengths of these catalysts.

These data are consistent with diffusion-enhanced secondary interconversions of primary alkylcyclopentene isomers (Scheme 1, Steps 5 and 6 shown for $12DMCP^=$ and $ECP^=$ interconversion) occurring within acid domains. These reactions are driven by intra-domain concentration gradients and occur before primary isomers can convert to their alkylcyclopentane analogs via hydrogen transfer locally at acid sites or via hydrogenation on Pt clusters present at the outer boundary of the acid domain (Scheme 1, Steps 7 and 8).

These diffusion-enhanced interconversions interfere with accurate assessments of intrinsic ring contraction selectivities ($S_{rc,P}$; “P” = ecp, 12, or 13 for ECP, 12DMCP, and 13DMCP). These intrinsic values rigorously reflect the ratio of the rate constants for the direct conversion of $MCH^=$ intermediates to each alkylcyclopentene isomer ($k_{rc,P}K_{p,mch}$) during one surface sojourn to their combined values as reflected in total $MCH^=$ conversion rates ($k_{rc}K_{p,mch}$):

$$S_{rc,P} = \frac{k_{rc,P}}{k_{rc}}, \tag{6}$$

It is such ratios that reflect the relative stabilities of the transition states that mediate each of these isomerization elementary events. In what follows, we relate measured selectivities shown in Figs. 3 and 4 to volumetric MCH conversion rates (Λ) by using diffusion–reaction treatments that also provide a method for extracting intrinsic (i.e., primary) selectivities to each ring contraction product and a predictive framework to describe selectivities observed in the practice of ring contraction catalysis.

The extent of secondary isomerization within acid domains determines, in part, the observed product selectivities. Their contributions depend on the volumetric density of protons within acid domains (ρ_a), on the proclivity of protons for catalyzing the isomerization of each alkylcyclopentene molecule (e.g. $k_{ecp\rightarrow12}K_{p,ecp}$ for $ECP^=$), and on the size and diffusive properties of the acid aggre-

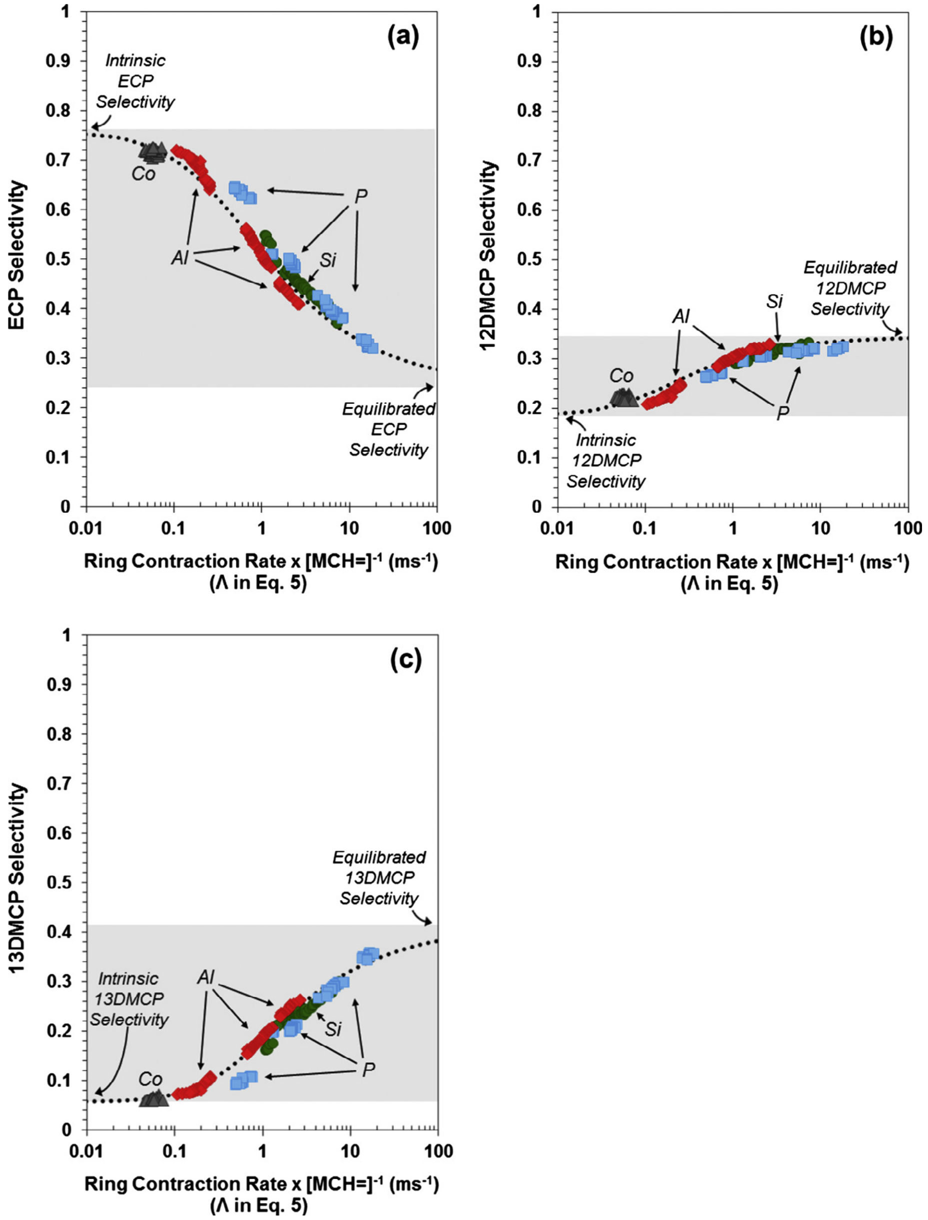

Fig. 4. Measured selectivities to (a) ethylcyclopentane, (b) 1,2-dimethylcyclopentane, and (c) 1,3-dimethylcyclopentane among ring contraction products from methylcyclohexane reactants ($S_{m,ecp}$, $S_{m,12}$, and $S_{m,13}$, respectively) as functions of the measured ring contraction rate per volume of catalyst normalized to the molar concentration of MCH$^{=}$ (Λ, Eq. (5)) on Pt/Al$_2$O$_3$ mixtures with H$_3$PW/SiO$_2$ ($Pt_S/H^+ = 5.4$, 0.022 H$^+$ (nm^3-SiO$_2$)$^{-1}$; ■), H$_4$SiW/SiO$_2$ ($Pt_S/H^+ = 3.3$, 0.018 H$^+$ (nm^3-SiO$_2$)$^{-1}$; ●), H$_5$AlW/SiO$_2$ ($Pt_S/H^+ = 1.7$, 0.020 H$^+$ (nm^3-SiO$_2$)$^{-1}$; ◆), and H$_6$CoW/SiO$_2$ ($Pt_S/H^+ = 38$, 0.002 H$^+$ (nm^3-SiO$_2$)$^{-1}$; ▲) (reaction conditions: 473 K, 191 – 442 kPa H$_2$). Dotted lines are best fits of the data to the functional form of Eq. (13). Shaded regions reflect the range of selectivities accessible to each of the products by changing Λ.

gates present in these bifunctional catalysts. The latter two properties of these aggregates determine the extent to which protons (where primary alkylcyclopentenes form) communicate with metal clusters (where they become less reactive by converting to alkylcyclopentanes), thus controlling the characteristic lifetimes of reactive alkylcyclopentene isomers before their conversion to less reactive alkylcyclopentanes. Such "site proximity" effects are seldom enforced or in fact rigorously known in the bound extrudates used in the practice of bifunctional metal–acid catalysis or even in impregnated bifunctional domains containing both acid and metal functions.

A more rigorous treatment of such diffusional constraints and of alkylcyclopentene isomer concentrations within acid domains requires diffusion–reaction formalisms that identify the relevant dimensionless parameters, in this case, the Thiele modulus (Φ). This parameter is defined for the ECP$^{=}$ consumption (Φ_{ecp}) pathways described in Scheme 1 as follows:

$$\Phi_{ecp}^2 = \frac{\rho_a R^2}{D_{ecp}}\left(\frac{k_{ecp\rightarrow 12}K_{p,ecp}}{1+K_{p,mch}K_{d,mch}\left(\frac{[MCH]}{[H_2]}\right)}\right) \qquad (7)$$

where R is the characteristic distance that defines the diffusion length within acid domains and D_{ecp} is the effective ECP$^{=}$ diffusivity within these acid domains. This treatment assumes the equilibration of MCH-H$_2$-MCH$^{=}$ and MCH$^{=}$-MCH*, as well as of alkylcyclopentenes with their respective alkoxides. It also considers the surface reactions that convert MCH* to C$_5$ ring alkoxides to be irreversible during a single visit to the active site and the isomerization of ECP* to 13DMCP* to occur only after the intervening conversion to one of the other alkoxide isomers because isomerizations events shift alkyl groups along backbones by one carbon at a time [10,21,25]. The Thiele moduli for 13DMCP$^{=}$ and 12DMCP$^{=}$ consumption via secondary reactions are related to that for ECP$^{=}$ consumption by the following:

$$\frac{\Phi_{13}^2}{\Phi_{ecp}^2} = \frac{D_{ecp}}{D_{13}}\left(\frac{k_{13\to12}K_{p,13}}{k_{ecp\to12}K_{p,ecp}}\right) = \frac{D_{ecp}}{D_{13}}\frac{K_{13,ecp}}{\sigma_{ecp}} \tag{8}$$

$$\frac{\Phi_{12}^2}{\Phi_{ecp}^2} = \frac{D_{ecp}}{D_{12}}\left(\frac{(k_{12\to ecp}+k_{12\to13})K_{p,12}}{k_{ecp\to12}K_{p,ecp}}\right) = \frac{D_{ecp}}{D_{12}}\left(\frac{1+\sigma_{ecp}}{\sigma_{ecp}}\right)K_{12,ecp} \tag{9}$$

Here, $K_{13,ecp}$ and $K_{12,ecp}$ are the equilibrium constants for 13DMCP$^{=}$-ECP$^{=}$ and 12DMCP$^{=}$-ECP$^{=}$ interconversions, D_{13} and D_{12} are the effective diffusivities for 13DMCP$^{=}$ and 12DMCP$^{=}$ within the mesoporous acid domains, and σ_{ecp} is the ratio of the rate constants for the surface elementary steps that convert 12DMCP* to ECP* and to 13DMCP* alkoxide isomers:

$$\sigma_{ecp} = \frac{k_{12\to ecp}}{k_{12\to13}}. \tag{10}$$

The Thiele moduli in Eqs. (7)–(9), and thus the alkylcyclopentene isomerization rate constants, cannot be determined directly from measured rates and selectivities, because of the ubiquitous diffusional corruptions of measured selectivities. Substituting Eq. (2) into Eq. (5) leads to an equation for methylcyclohexane ring contraction rates (to all alkylcyclopentanes) per acid domain volume divided by the MCH$^{=}$ concentration of (Λ); the resulting equation:

$$\Lambda = \frac{k_{rc}K_{p,mch}}{1+K_{p,mch}K_{d,mch}\left(\frac{[MCH]}{[H_2]}\right)}\rho_a \tag{11}$$

that is consistent with mechanism depicted in Scheme 1. Substituting Eq. (11) into Eq. (7) shows that for a given catalyst, the Thiele modulus for ECP$^{=}$ consumption (Φ_{ecp}; Eq. (7)) is proportional to $\Lambda^{1/2}$:

$$\Phi_{ecp} = \left(\Lambda\frac{R^2}{D_{ecp}}\left(\frac{k_{ecp\to12}K_{p,ecp}}{k_{rc}K_{p,mch}}\right)\right)^{1/2} = \Lambda^{1/2}\alpha_{ecp}^{1/2}. \tag{12}$$

The constant of proportionality in Eq. (12) (α_{ecp}) depends on the characteristic time for ECP$^{=}$ diffusion within the mesoporous acid aggregates (R^2/D_{ecp}) and on the ratio of the rate constant for ECP$^{=}$ isomerization to 12DMCP$^{=}$ ($k_{ecp\to12}K_{p,ecp}$) to that for MCH$^{=}$ ring contraction to all products ($k_{rc}K_{p,mch}$); it is independent of the volumetric density of H$^+$ within the acid domains, of the MCH or H_2 pressures, and of the relative magnitude of the two terms in the denominator of Eq. (2) (or Eq. (11)).

Next, we combine a kinetic treatment based on the elementary steps in Scheme 1 with the diffusion–reaction construct used to derive Eqs. (7)–(12) and their respective Thiele moduli to develop selectivity expressions for each of the alkylcyclopentene products. In what follows, equilibrium is assumed to prevail among MCH-H_2-MCH$^{=}$ gaseous molecules at the outer edge of acid domains, among all gaseous MCH$^{=}$ isomers and their respective MCH* alkoxides, and among all gaseous alkylcyclopentene isomers and their respective alkoxides. MCH* ring contraction steps are assumed to be irreversible and no direct ECP*-13DMCP* interconversion routes are taken into account; all alkylcyclopentenes are assumed to have the same diffusivity within the porous acid domains (a valid assumption in Knudsen or bulk diffusion regimes among molecules of the same mass [36]).

A kinetic-transport model based on these assumptions leads to selectivities ($S_{m,P}$) for each alkylcyclopentane isomer (derivation in Section SI.2., SI) given by the following:

$$S_{m,P} = S_{rc,P} + \Delta S_P(1-\eta_+) + \Theta_P(\eta_- - \eta_+) \tag{13}$$

where

$$\Delta S_P = \frac{K_{P,ecp}}{1+K_{12,ecp}+K_{13,ecp}} - S_{rc,P} \tag{14}$$

is the mole fraction of a given product "P" among the equilibrated pool of alkylcyclopentene products minus its intrinsic (kinetic) selectivity, Θ_P is a constant that is unique to each product "P" and reflects the changes in selectivity due to secondary influences (i.e. when η_+ is not equal to η_-; see Eqs. (15)–(18)), and η_+ and η_- are the effectiveness factors that describe the magnitude of the diffusional enhancements of secondary isomerization reactions within acid domains. The values of η_+ and η_- in Eq. (13) are the same for all products and depend on Φ_{ecp} (Eq. (7)) and ζ_+ or ζ_- (Eq. (16)) through the following:

$$\eta_+ = \frac{3(\zeta_+\Phi_{ecp}\coth(\zeta_+\Phi_{ecp})-1)}{\zeta_+^2\Phi_{ecp}^2} \quad \text{and}$$
$$\eta_- = \frac{3(\zeta_-\Phi_{ecp}\coth(\zeta_-\Phi_{ecp})-1)}{\zeta_-^2\Phi_{ecp}^2} \tag{15}$$

for the case of quasi-spherical acid domains, which can be generalized to other shapes according to their associated shape factors [37]. The parameters ζ_+ and ζ_- in Eq. (15) depend only on σ_{ecp}, $K_{13,ecp}$ and $K_{12,ecp}$:

$$\begin{aligned}\zeta_\pm^2 = {} & \frac{1}{2}\left(1+\frac{(1+\sigma_{ecp})}{\sigma_{ecp}}K_{12,ecp}+\frac{K_{13,ecp}}{\sigma_{ecp}}\right)\\ & \pm\frac{1}{2}\sqrt{1+\left(\frac{(1+\sigma_{ecp})}{\sigma_{ecp}}K_{12,ecp}\right)^2+\left(\frac{K_{13,ecp}}{\sigma_{ecp}}\right)^2+2\frac{K_{12,ecp}}{\sigma_{ecp}}\left(\frac{K_{13,ecp}}{\sigma_{ecp}}+\sigma_{ecp}-(1+K_{13,12}+K_{13,ecp})\right)}\end{aligned} \tag{16}$$

Eq. (13) depends on two effectiveness factors (η_+ and η_-) because secondary isomerization reactions occur via two distinct routes: 12DMCP*-ECP* and 12DMCP*-13DMCP* interconversions (Scheme 1, Step 6a and 6b). The choice of the modulus for ECP$^{=}$ (Φ_{ecp}) in Eq. (15), instead of those for 12DMCP$^{=}$ or 13DMCP$^{=}$, is arbitrary, because all moduli merely differ by a constant factor (Eqs. (8) and (9)); the alternate use of Φ_{12} or Φ_{13} would change the form and values of ζ_+ and ζ_-, but not those for η_+ or η_-. The Θ_P term in Eq. (13) influences selectivities for intermediate η values (Eq. (12)) and its magnitude depends on σ_{ecp}, $K_{13,ecp}$, and $K_{12,ecp}$, and on ΔS_P for two of the three ring contraction products (the third given by difference). In the case of ECP$^{=}$ this relation is as follows:

$$\Theta_{ecp} = \left(\zeta_-^2-\frac{K_{13,ecp}}{\sigma_{ecp}}\right)\frac{\sigma_{ecp}\,\Delta S_{13}\left(\zeta_+^2-\frac{K_{13,ecp}}{\sigma_{ecp}}\right)-\Delta S_{ecp}(\zeta_+^2-1)}{\left(1-\frac{K_{13,ecp}}{\sigma_{ecp}}\right)(\zeta_+^2-\zeta_-^2)} \tag{17}$$

The Θ_P value for 13DMCP$^{=}$ is proportional to that for ECP$^{=}$:

$$\frac{\Theta_{13}}{\Theta_{ecp}} = \frac{\zeta_{-}^{2} - 1}{\sigma_{ecp}\left(\zeta_{-}^{2} - \frac{K_{13,ecp}}{\sigma_{ecp}}\right)} \tag{18}$$

while that for 12DMCP$^{=}$ (Θ_{12}) is simply given by their sum ($\Theta_{12} = -(\Theta_{ecp} + \Theta_{13})$). Eqs. (13)–(18) predict that observed selectivities (at differential conditions) depend on the intrinsic selectivities for ring contraction products ($S_{rc,P}$), but also on the thermodynamic and kinetic constants for alkylcyclopentene interconversions and on the characteristic diffusion time within acid domains (R^2/D).

Eqs. (11) and (12) also indicate that measured total volumetric rates of MCH conversion divided by [MCH$^{=}$] concentrations (defined as Λ in Eq. (5)) reflect the activity per acid domain volume and the kinetic constants for interconversion of alkylcyclopentenes. The dashed curves in Fig. 3b and the dotted curves in Fig. 4a–c depict the regressed fits of the selectivity data in Fig. 4 at all MCH and H_2 pressures on the H_nXW/SiO_2-Pt/Al_2O_3 catalyst mixtures with P, Si, Co and Al central atoms to the functional form of Eq. (13). In such a regression, the six independent parameters in Eqs. (12)–(18) ($S_{rc,ecp}/S_{rc,12}$, $S_{rc,13}/S_{rc,12}$, $K_{12,ecp}$, $K_{12,ecp}$, α_{ecp}, and σ_{ecp}) are kept the same for all POM compositions and are listed in Table 3. The shaded regions in Fig. 4(a–c) reflect the range of accessible selectivities prescribed by Eq. (13) (given that effectiveness factors range from 0 to 1) for each product according to the values of the fitted parameters in Table 3. These accessible selectivities are bound by extrema defined by thermodynamics and by intrinsic kinetics, as we discuss below.

The regressed values of ($S_{rc,ecp}/S_{rc,12}$) and ($S_{rc,13}/S_{rc,12}$) (Table 3) indicate that the non-branching ECP product is the predominant primary products of MCH$^{=}$ isomerization ($S_{rc,ecp} = 0.76$; $S_{rc,12} = 0.18$; $S_{rc,13} = 0.06$), suggesting that the TS that mediates ECP* formation is more stable than those involved in 12DMCP* and 13DMCP* formation from MCH*. These results are consistent with non-branching C_6 alkene isomerization events also being more facile than those that lengthen or shorten their backbone [10,25] and with non-branching TS having more substituted and, consequently more stable, cyclopropyl structures than branching TS [2,26,38]. The fitted values of $K_{12,ecp}$ and $K_{13,ecp}$ are near unity (0.70 and 0.58, respectively; Table 3) indicating the concentrations of lumped cycloalkenes with a given backbone (either ECP, 12DMCP, or 13DMCP backbones) and equilibrated alkene regioisomers are similar at equilibrium. Values of σ_{ecp} near unity ($\sigma_{ecp} = 0.90$) are indicative of similar TS free energies for 12DMCP*-ECP* and 12DMCP*-13DMCP* interconversions [26].

Diffusion through porous solids consisting of quasi-spherical packings within domains occurs with effective Knudsen diffusivities (D_{eA}) that depend on the void fraction (ϕ), tortuosity factor (τ), and surface area per unit volume (a_v) of these solids [39]:

$$D_{eA} = \frac{4}{3}\frac{\phi^2}{\tau a_v}\left(\frac{8\bar{R}T}{\pi M_A}\right)^{1/2} \tag{19}$$

where M_A is the molecular weight of the diffusing molecule. Here, we surmise that acid domains retain the approximate diameter of the POM/SiO_2 aggregates mixed with Pt/Al_2O_3 (~20 μm). The SiO_2 support has a surface area per volume of 0.21 nm^{-1} and a void fraction of 0.4; the tortuosity factor for spherical packings with this void fraction is ~3 [40]. For these values, Eq. (19) gives an ECP$^{=}$ characteristic diffusion time (0.6 ms; R^2/D_{ecp}, Eq. (12)) much smaller than regressed α_{ecp} values (Eq. (12)) (30.8 ms); according to Eq. (12), this corresponds to rate constants for ECP$^{=}$ conversion to 12DMCP$^{=}$ ($k_{ecp\rightarrow12}K_{p,ecp}$) that are ~ 50 times larger than those for MCH$^{=}$ conversion to all ring contraction products ($k_{rc}K_{p,mch}$). Diffusional effects influence selectivities, but not MCH ring contraction rates, because ECP$^{=}$, 12DMCP$^{=}$, and 13DMCP$^{=}$ have much shorter characteristic times for isomerization reactions ($(k_{R\rightarrow P}K_{p,R})^{-1}$) than MCH$^{=}$ ($(k_{rc}K_{p,mch})^{-1}$), but similar characteristic diffusion times (R^2/D) as a result of the similar mass of the diffusing molecules. Consequently, the Thiele moduli for the consumption of ECP$^{=}$, 12DMCP$^{=}$, and 13DMCP$^{=}$ via secondary reactions are much larger than that for the primary ring contraction reactions of MCH$^{=}$.

Table 3
Values of the parameters from Eqs. (12)–(18) determined by regression of all the data in Fig. 4(a–c) to the functional form of Eq. (13).

α_{ecp}	30.8 ms		
σ_{ecp}	0.90		
$K_{12,ecp}$	0.70		
$K_{13,ecp}$	0.58		
$S_{rc,ecp}/S_{rc,12}$	4.20		
$S_{rc,13}/S_{rc,12}$	0.31		
	ECP$^{=}$	*12DMCP*$^{=}$	*13DMCP*$^{=}$
Intrinsic selectivity ($S_{rc,P}$)	0.76	0.18	0.06
Thermodynamic selectivity ($S_{rc,P} + \Delta S_P$)	0.28	0.35	0.37
Θ_P	0.40	0.04	−0.44

The data in Fig. 4 suggest that for a given acid domain size, proton density, and diffusive properties, acid strength influences the measured selectivities, but not those for the formation of each primary product (i.e. the intrinsic selectivity). Acid strength affects the rate constants for the surface elementary steps that interconvert 12DMCP*, ECP*, and 13DMCP* to the same extent (i.e. σ_{ecp} in Eq. (10) is the same for all POM acids), but in doing so leads to larger Thiele moduli on stronger acids (Φ_{ecp}, Eq. (7)). As a result stronger acids cause greater diffusional enhancements of secondary interconversions (given by η_{+} and η_{-}; Eq. (15)), even though the relative rates of alkylcyclopentoxide formation and of their secondary interconversions are not sensitive to acid strength. The form of Eq. (12) and the data in Fig. 4 show that larger Φ_{ecp} values bring products closer to the relative abundance prescribed by thermodynamics. Asymptotic selectivities for small Φ_{ecp} values reflect instead the intrinsic rates of MCH$^{=}$ ring contraction to form each product in a single sojourn at a proton. These trends and conclusions remain valid irrespective of which specific parameters lead to a change in the value of Φ_{ecp}. These parameters include the distance between metal and acid sites (because metal sites define the boundary of acid domains) (R), the difficulty in traversing the intervening path between metal and acid functions (D_{ecp}), and the number of protons that reside within that path (ρ_a). Diffusional enhancements of secondary interconversions become weaker as MCH$^{=}$ concentrations increase and protons approach saturation coverages of methylcyclopentoxides ($K_{p,mch}[MCH^{=}]$), because effective rate constants ($r_{rc}/[MCH^{=}]$) are lower at saturation than in the first-order kinetic regime. This is not directly evident from our treatment, because it focuses on the first-order kinetic regime where MCH$^{=}$ and its products react on sparsely occupied protons to allow closed-form solutions.

We note that these diffusion-enhanced secondary interconversions have led to the inaccurate attribution of differences in selectivities among catalysts to acid strength effects and to the incorrect conclusions that (i) more demanding reactions are kinetically favored on stronger acids and (ii) microporous acids contain protons of greater acid strength than mesoporous aluminosilicates. In fact, the rates of formation of all alkylcyclopentene isomers (and isohexene isomers [10]) are similarly affected by acid strength. Stronger acids and confinement effects both increase the magnitude of all isomerization rate constants, thus increasing the contributions from secondary interconversions through their effects on Thiele moduli; such interconversions always bring selectivities closer to their thermodynamic values, causing the isomers formed in more kinetically-demanding reactions to form at the expense of those formed in the more facile steps. Microporous solids additionally impose stronger diffusional barriers; thus,

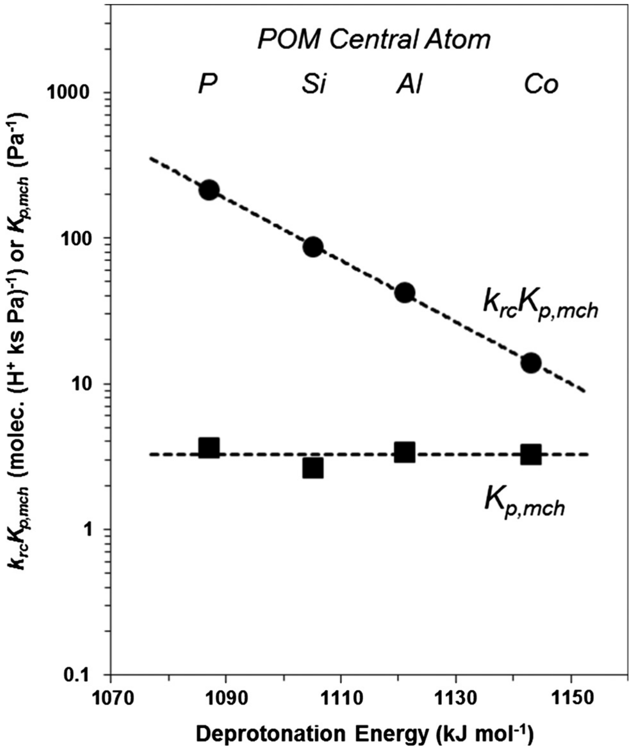

Fig. 5. Measured methylcyclohexene ring contraction rate constants to form all isomers ($k_{rc}K_{p,mch}$; ●) and equilibrium constants for MCH$^=$ protonation to MCH* ($K_{p,mch}$; ■) using methylcyclohexane reactants for H_nXW/SiO_2(X = P, Si, Al, Co) (473 K) mixtures with Pt/Al_2O_3 as a function of their deprotonation energies. The upper dashed line is the regressed linear fit of the measured $k_{rc}K_{p,mch}$ values and the lower dashed line is the average of the four $K_{p,mch}$ values.

Thiele moduli are larger and the extent of secondary interconversions is even more significant.

Such effects of confinement and acid strength merely reflect the predominant initial formation of the "facile" isomer and the diffusion-enhanced secondary interconversions that move products in the direction of their thermodynamic prevalence. The phenomenological use of selectivity in probe reactions to assess the acid strength of materials, even at differential conversion, is therefore inappropriate without considering the ancillary complexities of diffusional constraints; in fact, the sought-after kinetic selectivities are insensitive to acid strength and, in the absence of specific transition state stabilization, also to confinement effects. Such measurements provide a scale to assess acid strength only when these diffusional effects are absent, which seems seldom the case for bifunctional isomerization reactions, as shown here for cycloalkanes (and in [10] for acyclic alkanes), or when their effects are rigorously described by kinetic-transport models, such as that reported in this study, but not previously used in the analysis of isomerization selectivities. In Section 3.2 we show how the acid strength effects on the rate constants for the formation of each primary MCH$^=$ conversion product can be determined from measured selectivities using these kinetic-transform models.

3.2. Acid strength effects on methylcyclohexene ring contraction rates

The ability to extract intrinsic rate constants for individual MCH* isomerization steps from measured selectivities using the kinetic-transport formalisms described here allows a rigorous assessment of the effects of acid strength on each of the rate constants for these elementary steps by using POM clusters with different central atoms and DPE values and known numbers of accessible protons.

Fig. 5 shows $k_{rc}K_{p,mch}$ and $K_{p,mch}$ values on each POM/SiO_2-Pt/Al_2O_3 mixture (regressed from the data in Fig. 1 to the functional form of Eq. (2)) as a function of their DPE values [7]. POM clusters with higher-valent central atoms (and fewer protons) exhibit smaller DPE values, because their lower electron density leads to more stable conjugate anions. Values of $k_{rc}K_{p,mch}$ increase exponentially with decreasing DPE values (Fig. 5), indicative of stronger acid sites, because ion-pairs at relevant ring contraction transition states for all isomerization steps (see Section 3.2) benefit from the more stable conjugate anions in the stronger acids. In contrast, $K_{p,mch}$ values are essentially insensitive to DPE because methylcyclohexoxides are similarly charged as unoccupied protons and are thus not affected by the stability of conjugate anions [26].

Scheme 2 depicts the reaction coordinate for MCH$^=$ ring contraction on Brønsted acid sites and the individual free energy terms that account for the measured activation free energy barriers for the lumped kinetic parameter ($k_{rc}K_{p,mch}$). In the formalism of transition state theory, free-energy barriers for $k_{rc}K_{p,mch}$ ($\Delta G^{\ddagger}_{app}$ in Scheme 2) include the free energies required (i) to protonate the lumped (and equilibrated) gaseous MCH$^=$ isomers to form MCH* lumped alkoxide species, in which attachment positions to the O-atoms are also in equilibrium ($\Delta G_{p,mch}$ in Scheme 2) and (ii) to rearrange MCH* species to form the ensemble of TS structures that mediate ring contraction events from an equilibrated mixture of adsorbed MCH* alkoxides ($\Delta G^{\ddagger}_{rc}$ in Scheme 2). The $k_{rc}K_{p,mch}$ value, in turn, reflects the combined additive contributions of the rate constants to form ring contraction products ($\sum_P k_{rc,P}K_{P,mch}$, Eq. (3)); as a result, $\Delta G^{\ddagger}_{app}$ reflects the combined contributions of the free energies of all ring contraction TS structures ($G^{\ddagger}_{mch\leftrightarrow P}$ in Scheme 2) relative to those for lumped gaseous MCH$^=$ isomers and to an uncovered H$^+$ (G_{mch} in Scheme 2) averaged exponentially because of the exponential dependence of rate constants on free energies:

$$\Delta G^{\ddagger}_{app} = -RT\ln\left(\sum_P \exp\left(\frac{-(G^{\ddagger}_{mch\leftrightarrow P} - G_{mch})}{RT}\right)\right) = -RT\ln\left(\sum_P \exp\left(\frac{-\Delta G^{\ddagger}_{app,P}}{RT}\right)\right) \quad (20)$$

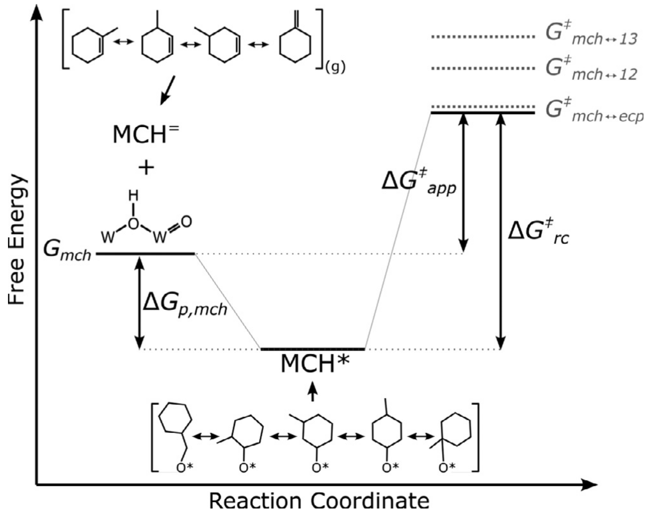

Scheme 2. Reaction coordinate diagram depicting the free energies of MCH$^=$ and MCH* regioisomer groups and the free energies of the ring contraction transition states accessible to MCH*. Free-energy barriers for $k_{rc}K_{p,mch}$ ($\Delta G^{\ddagger}_{rc,app}$) and k_{rc} ($\Delta G^{\ddagger}_{rc}$) and the free-energy difference for $K_{p,mch}$ ($\Delta G_{p,mch}$) are also shown.

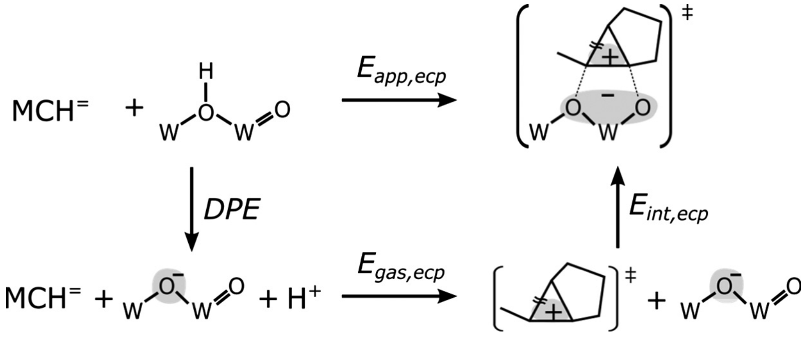

Scheme 3. Thermochemical cycle for formation of the ring contraction transition state leading to ethylcyclopentene on POM acid catalysts.

The observed exponential effects of DPE on $k_{rc}K_{p,mch}$ can then be interpreted by taking derivatives using Eq. (20):

$$-RT\frac{d(\ln(k_{rc}K_{p,mch}))}{d(DPE)} = \frac{d(\Delta G^{\ddagger}_{app})}{d(DPE)} = \sum_{P} S_{rc,P}\frac{d(\Delta G^{\ddagger}_{app,P})}{d(DPE)} \qquad (21)$$

in which $\Delta G^{\ddagger}_{app,P}$ is the apparent free-energy barrier to form the specific transition state responsible for the formation of the ring contraction product "P" and $S_{rc,P}$ is the intrinsic primary selectivity to form product "P" from MCH$^=$.

The right side of Eq. (21) shows that measured $d(\Delta G^{\ddagger}_{app})/d(DPE)$ values reflect the selectivity-weighed mean value of the derivatives in Eq. (21) for each ring contraction product P. Ring contraction TS structures are similar on POM clusters with different central atom [10,21,26]; consequently, $d(\Delta G^{\ddagger}_{app})/d(DPE)$ values predominantly reflect concomitant effects of DPE on activation energies, because of their similar activation entropies [7,21] and Eq. (21) becomes the following:

$$-RT\frac{d(\ln(k_{rc}K_{p,mch}))}{d(DPE)} = \frac{d(E_{app})}{d(DPE)} = \sum_{P} S_{rc,P}\frac{d(E_{app,P})}{d(DPE)} \qquad (22)$$

Here, E_{app} and $E_{app,P}$ are the respective apparent activation barriers for $k_{rc}K_{p,mch}$ and the $k_{rc,P}K_{p,mch}$ terms for each product "P". The linear dependence of $\ln(k_{rc}K_{p,mch})$ on DPE (Fig. 5) demonstrates that $d(E_{app})/d(DPE)$ is a constant for the range of DPE values in Fig. 5, making its value insensitive to acid strength for POM clusters differing significantly in reactivity ($k_{rc}K_{p,mch}$; 15-fold). Measured $d(E_{app})/d(DPE)$ values (0.19; Fig. 5) are much smaller than unity, indicating that E_{app} increases less than the accompanying changes in DPE and that ring contraction transition states partially attenuate the effects of changes in DPE on activation barriers. The form of Eq. (22) requires that the stability of all ring contraction TS depends similarly on DPE (with $d(E_{app,P})/d(DPE) = 0.19$ for all products) for $d(E_{app})/d(DPE)$ values not to sense the significant changes in DPE among these POM clusters. As a result, intrinsic ring contraction selectivities ($S_{rc,P}$) cannot depend on DPE (and acid strength), consistent with measured selectivities that are accurately described using the same intrinsic selectivities for all POM (dashed curves; Fig. 4).

Born-Haber thermochemical cycles provide instructive constructs that allow activation barriers for acid catalysis [41] to be dissected into those for hypothetical steps that independently sense properties of the catalyst (e.g., DPE) and of the molecules (e.g. proton affinities of gaseous species) [10,21,42–44]. Specifically, activation barriers for MCH$^=$ conversion to ECP$^=$ include hypothetical steps (Scheme 3) that (i) deprotonate the POM cluster (DPE); (ii) react a gaseous H$^+$ with MCH$^=$(g) to form a gaseous analog of the cation at the TS ($E_{gas,ecp}$); and (iii) allow the gaseous TS analog to interact with the POM conjugate anion to form the ion-pair transition state for ring contraction ($E_{int,ecp}$):

$$E_{app,ecp} = DPE + E_{gas,ecp} + E_{int,ecp} \qquad (23)$$

Thus, DPE effects on $E_{app,ecp}$ reflect solely the effects of DPE on $E_{int,ecp}$, which are determined, in turn, by the extent to which the interactions of the TS cation with the conjugate anion recover the energy required to deprotonate the POM acids. Such interactions recover a large fraction of the ionic component of DPE values (the classical electrostatic interactions as ions move relative to one another), but a much smaller fraction of covalent component in DPE (any reorganization, structural or electronic, induced by the proximity of two species at their equilibrium distances) [45].

The replacement of $E_{app,P}$ in Eq. (22) with the analog of Eq. (23) for each ring contraction product P leads to a relation between $k_{rc}K_{p,mch}$ values and DPE:

$$\frac{d(E_{app})}{d(DPE)} = 1 + \sum_{P} S_{rc,P}\frac{d(E_{int,P})}{d(DPE)} \qquad (24)$$

The individual $d(E_{gas,P})/d(DPE)$ term for each product P is absent because $E_{gas,P}$ is a property of gaseous species (Eq. (19)). In Section 3.1, we showed that intrinsic MCH$^=$ ring contraction selectivities ($S_{rc,P}$ in Eq. (24)) did not depend on DPE. The $\ln(k_{rc}K_{p,mch})$ values depend linearly on DPE (Fig. 5), confirming that neither $d(E_{app})/d(DPE)$ nor any of the terms in the summation of Eq. (24) depend on DPE. We conclude, as inferred earlier, that $E_{int,P}$ values and MCH$^=$ ring contraction TS energies for all products depend similarly on DPE. Eq. (24) then becomes the following:

$$\frac{d(E_{app})}{d(DPE)} = 1 + \frac{d(E_{int,P})}{d(DPE)} \qquad (25)$$

The $d(\ln(k_{rc}K_{p,mch}))/d(DPE)$ value from the data in Fig. 5 (at 473 K) corresponds to a $d(E_{int,P})/d(DPE)$ value of −0.8, indicating that each ring contraction TS recovers 80% of difference in DPE among these acids. Their absolute values are smaller than unity because the small and highly localized charges in gaseous protons lead to stronger interactions with POM conjugate anions than those for TS gaseous analogs. The similar effects of DPE on the stability of ion-pairs that mediate the different ring contraction events indicate that the charge is similarly distributed throughout their respective organic cations.

4. Conclusions

The effects of acid strength on reactivity and of acid strength and site proximity on selectivity are demonstrated using methylcyclohexane ring contraction reactions on well-defined solid Brønsted acids in mixtures with Pt/Al$_2$O$_3$ co-catalysts. When present in sufficient amounts, metal sites equilibrate dehydrogenation/hydrogenation reactions of reactant and product alkanes/alkenes and provide a low and constant concentration of alkenes outside of all acid domains. Measured rate data were interpreted mechanistically in order to determine rate constants for the total rate of methylcyclohexene ring contraction ($k_{rc}K_{p,mch}$) normalized to the number of reactive H$^+$ on Keggin POM clusters. These rate constants reflect the stabilities of ion-pair transition states, which mediate kinetically-relevant methylcycloalkoxide ring contraction steps, relative to an equilibrated lump of gaseous reactant methylcyclohexenes and unoccupied acid sites. Activation barriers for ring contraction reactions to all products increase with increasing DPE on Keggin POM because cationic organic fragments at all ring contraction transition states recover only a portion of the additional energy required to deprotonate weaker acids.

Measured ring contraction selectivities at differential methylcyclohexane conversions depend only on the total ring contraction rate per volume of catalyst divided by [$\text{MCH}^{=}$] (a surrogate for the density and activity of acid sites in acid domains) on Keggin POM clusters supported on mesoporous SiO_2. This reflects intrinsic ring contraction selectivities for branched and un-branched products and those for secondary isomerizations that interconvert ring contraction products that are independent of acid strength. Changes in acid strength affect measured ring contraction selectivities only when such changes also change the value of the Thiele moduli for $\text{ECP}^{=}$ consumption (Φ_{ecp}) and, concomitantly, the extent of secondary isomerization reactions among ring contraction products within acid domains, not by changing the relative rates of alkylcyclopentoxide formation from methylcyclohexene at acid sites. At low values of Φ_{ecp}, measured selectivities approach those predicted by the intrinsic rates of alkylcyclopentoxide formation from methylcyclohexene, and at high values, measured selectivities approach those predicted for an equilibrated mixture of alkylcyclopentene products. Such effects are expected for any change in catalyst property that changes Φ_{ecp}. Consequently, increasing site proximity among metal and acid sites, which decreases the characteristic length of the acid domain; decreasing density of acid sites in the acid domain; increasing the diffusivity of products in the catalyst support, decreasing the fraction of uncovered acid sites covered; or decreasing the acid strength of the catalyst will all shift measured selectivities in the same direction: toward those predicted by the intrinsic rates of alkylcyclopentoxide formation from methylcyclohexene.

Appendix A. Nomenclature

Symbol	Unit	Definition
$\text{12DMCP}^{=}$, $\text{13DMCP}^{=}$, $\text{ECP}^{=}$, $\text{MCH}^{=}$	–	Lumped chemical pseudo-species made up of alkene regioisomers that share the same carbon skeleton and only differ in the position of the double bond
12DMCP^{*}, 13DMCP^{*}, ECP^{*}, MCH^{*}	–	Lumped chemical pseudo-species made up of alkoxide regioisomers that share the same carbon skeleton and only differ in the position of the surface attachment
a_v	nm^{-1}	Surface area per unit volume of a solid
D_P	m^2/s	Effective diffusivity of product "P" ("P" = ecp, 12, or 13 for $\text{ECP}^{=}$, $\text{12DMCP}^{=}$, and $\text{13DMCP}^{=}$, respectively) in the mesoporous acid aggregate (here silica)
DPE	kJ mol^{-1}	Energy required to deprotonate an acid (Scheme 3)
E_{app}	kJ mol^{-1}	Apparent activation barrier for $k_{rc}K_{p,mch}$
$E_{app,P}$	kJ mol^{-1}	Apparent activation barrier for the $k_{rc,P}K_{p,mch}$ term for product "P" (Scheme 3)
$E_{gas,P}$	kJ mol^{-1}	Energy required to react a gaseous H^+ with $\text{MCH}^{=}$ to form a gaseous analog of the cation at the TS that mediates the formation of ring contraction product "P" (Scheme 3)
$E_{int,P}$	kJ mol^{-1}	Energy associated with the interaction of the gaseous analog of the cation at the TS that mediates the formation of ring contraction product "P" with the POM conjugate anion when forming the ion-pair TS (Scheme 3)
G_{mch}	kJ mol^{-1}	Free energy of the $\text{MCH}^{=}$ regioisomer group and an uncovered acid site (Scheme 2)
$\text{G}^{\ddagger}_{mch\leftrightarrow P}$	kJ mol^{-1}	Free energy of the TS mediating the formation of ring contraction product "P" (Scheme 2)
$K_{d,mch}$	Pa	Equilibrium constant for MCH dehydrogenation to $\text{MCH}^{=}$
$K_{p,mch}$	Pa^{-1}	Equilibrium constant for $\text{MCH}^{=}$ protonation to MCH^{*}
$K_{p,P}$	Pa^{-1}	Equilibrium constant for product "P" protonation. ("P" = ecp, 12, or 13 for $\text{ECP}^{=}$ to ECP^{*}, $\text{12DMCP}^{=}$ to 12DMCP^{*}, and $\text{13DMCP}^{=}$ to 13DMCP^{*}, respectively)
$K_{P,P'}$	–	Equilibrium constant for the equilibration of product "P" and product "P" ("P" or "P" = ecp, 12, or 13 for $\text{ECP}^{=}$, $\text{12DMCP}^{=}$, and $\text{13DMCP}^{=}$, respectively)
$k_{P\rightarrow P'}$	molec. $(\text{H}^+\ \text{ks})^{-1}$	Rate constant for "P" isomerization to product "P" ("P" or "P" = ecp, 12, or 13 for ECP^{*}, 12DMCP^{*}, and 13DMCP^{*}, respectively)
k_{rc}	molec. $(\text{H}^+\ \text{ks})^{-1}$	Rate constant for MCH^{*} ring contraction to all products
$k_{rc,P}$	molec. $(\text{H}^+\ \text{ks})^{-1}$	Rate constant for MCH^{*} ring contraction to product "P"
M_A	kg mol^{-1}	Molecular weight of species A
R	m	Characteristic length of acid domains
$\bar{R}$	$\text{kg m}^2\ \text{mol}^{-1}\ \text{K}^{-1}\ \text{s}^{-2}$	Ideal gas constant
r_{rc}	molec. $(\text{H}^+\ \text{ks})^{-1}$	Rate of MCH ring contraction to all alkylcyclopentane isomers
$r_{rc,P}$	molec. $(\text{H}^+\ \text{ks})^{-1}$	Rate of MCH ring contraction to product "P"
$S_{m,P}$	–	Measured selectivity to product "P"
$S_{rc,P}$	–	Intrinsic MCH^{*} ring contraction selectivity to product "P"
V_{cat}	m^3	Total volume of the acid catalyst
α_{ecp}	ms	Ratio of the Thiele modulus for $\text{ECP}^{=}$ consumption to Λ
$\Delta G^{\ddagger}_{app}$	kJ mol^{-1}	Free-energy barrier for $k_{rc}K_{p,mch}$ (Scheme 2)
$\Delta G^{\ddagger}_{rc}$	kJ mol^{-1}	Free-energy barrier for k_{rc} (Scheme 2)
$\Delta G_{p,mch}$	kJ mol^{-1}	Free-energy difference for $K_{p,mch}$ (Scheme 2)

Appendix A (*continued*)

Symbol	Unit	Definition
ζ_+ and ζ_-	–	Constants that relate the Thiele modulus for $ECP^=$ consumption to those for all secondary isomerization reactions. The values of these constants depend explicitly on σ_{ecp} and $S_{eq,P}$
η_+ and η_-	–	Effectiveness factors that describe the extent of secondary isomerization reactions within acid domains
τ	–	The void fraction of a solid
Θ_P	–	A constant unique to product "P" that affects selectivities to product "P" when η_+ and η_- are between extremes
ϕ	–	Tortuosity factor of a solid
Λ	ms^{-1}	Rate of MCH ring contraction to all alkylcyclopentane isomers per volume of acid catalyst divided by the concentration of $MCH^=$
ρ_a	$H^+ (nm^3\text{-}SiO_2)^{-1}$	Volumetric density of Brønsted acid sites in acid domains
σ_{ecp}	–	Ratio of the rate constant for $12DMCP^*$ isomerization to ECP^* over that for $12DMCP^*$ isomerization to $13DMCP^*$
Φ_P^2	–	Thiele modulus for consumption of product "P" via secondary isomerization reactions

Acknowledgments

The support by the Chemical Sciences, Geosciences, Biosciences Division, Office of Basic Energy Sciences, Office of Science, U.S. Department of Energy under grant number DE-AC05-76RL0-1830 is appreciatively acknowledged. W.K. acknowledges with thanks the Chevron Fellowship granted in partial support of this research. The authors would like to thank Dr. Prashant Deshlahra (UC-Berkeley) for insightful discussions. We also thank Dr. Cindy Yin (UC-Berkeley) and Dr. Stuart Soled (ExxonMobil) for their assistance with the synthesis of unsupported $H_5AlW_{12}O_{40}$.

Appendix B. Supplementary material

Supplementary data associated with this article can be found, in the online version, at http://dx.doi.org/10.1016/j.jcat.2016.08.007.

References

[1] T. Prasomsri, S. Jongpatiwut, M. Santikunaporn, D.E. Resasco, Selectivity of Ring-Contraction Products in the Hydroisomerization of Methylcyclohexane, in: 2007 Spring Meet. 3rd Glob. Congr. Process Saf. 10th Top. Conf. Refin. Process., Houston, 2007.

[2] G.B. McVicker, O.C. Feeley, J.J. Ziemiak, D.E.W. Vaughan, K.C. Strohmaier, W.R. Kliewer, et al., Methylcyclohexane ring-contraction: a sensitive solid acidity and shape selectivity probe reaction, J. Phys. Chem. B 109 (2005) 2222–2226, http://dx.doi.org/10.1021/jp040205k.

[3] C. Nguyen, C. Sonwane, S. Bhatia, D. Do, Adsorption of benzene and ethanol on MCM-41 material, Langmuir 7463 (1998) 4950–4952.

[4] E.G. Derouane, J.C. Védrine, R.R. Pinto, P.M. Borges, L. Costa, M.A.N.D.A. Lemos, et al., Measurements and relation to catalysis: a review on experimental and theoretical methods for the study of zeolite acidity, Catal. Rev. 55 (2013) 454–515, http://dx.doi.org/10.1080/01614940.2013.822266.

[5] H.F. Uhlig, W.C. Pfefferle, The octafining process for isomerization of C8 aromatics containing ethylbenzene, in: L. Spillane, H. Leftin (Eds.), Refin. Pet. Chem., American Chemical Society, Newark, 1970, pp. 204–214, http://dx.doi.org/10.1021/ba-1970-0097.ch012.

[6] H. Abrevaya, Unique aspects of mechanisms and requirements for zeolite catalysis in refining and petrochemicals, in: S. Kulprathipanja (Ed.), Zeolites Ind. Sep. Catal., Wiley-VCH Verlag GmbH & Co. KGaA, Weinheim, Germany, 2010, pp. 403–478, http://dx.doi.org/10.1002/9783527629565.ch13.

[7] J. Macht, M.J. Janik, M. Neurock, E. Iglesia, Mechanistic consequences of composition in acid catalysis by polyoxometalate Keggin clusters, J. Am. Chem. Soc. 130 (2008) 10369–10379, http://dx.doi.org/10.1021/ja803114r.

[8] J. Macht, M.J. Janik, M. Neurock, E. Iglesia, Catalytic consequences of composition in polyoxometalate clusters with Keggin structure, Angew. Chem. Int. Ed. 46 (2007) 7864–7868, http://dx.doi.org/10.1002/anie.200701292.

[9] M.J. Janik, J. Macht, E. Iglesia, M. Neurock, Correlating acid properties and catalytic function: a first-principles analysis of alcohol dehydration pathways on polyoxometalates, J. Phys. Chem. C 113 (2009) 1872–1885, http://dx.doi.org/10.1021/jp8078748.

[10] W. Knaeble, R.T. Carr, E. Iglesia, Mechanistic interpretation of the effects of acid strength on alkane isomerization turnover rates and selectivity, J. Catal. 319 (2014) 283–296, http://dx.doi.org/10.1016/j.jcat.2014.09.005.

[11] R.T. Carr, M. Neurock, E. Iglesia, Catalytic consequences of acid strength in the conversion of methanol to dimethyl ether, J. Catal. 278 (2011) 78–93, http://dx.doi.org/10.1016/j.jcat.2010.11.017.

[12] W.J. Knaeble, E. Iglesia, Kinetic and theoretical insights into the mechanism of alkanol dehydration on solid Brønsted acid catalysts, J. Phys. Chem. C (2016), http://dx.doi.org/10.1021/acs.jpcc.5b11127 acs.jpcc.5b11127.

[13] H.S. Cerqueira, P.C. Mihindou-Koumba, P. Magnoux, M. Guisnet, Methylcyclohexane transformation over HFAU, HBEA, and HMFI zeolites: I. Reaction scheme and mechanisms, Ind. Eng. Chem. Res. 40 (2001) 1032–1041, http://dx.doi.org/10.1021/ie000730f.

[14] M. Santikunaporn, W.E. Alvarez, D.E. Resasco, Ring contraction and selective ring opening of naphthenic molecules for octane number improvement, Appl. Catal. A Gen. 325 (2007) 175–187, http://dx.doi.org/10.1016/j.apcata.2007.03.029.

[15] J. Cowan, C.L. Hill, R. Reiner, I. Weinstock, Dodecatungstoalumic acid and its monolacunary & mixed-addendum derivatives, Inorg. Synth. 33 (2002) 18–26.

[16] L. Baker, B. Loev, T. McCutcheon, Hydrogen cycle cation exchange for heteropoly acids and salts*, J. Am. Chem. Soc. 72 (1950) 2374–2377.

[17] L. Baker, T. McCutcheon, Heteropoly salts containing cobalt and hexavalent tungsten in the anion1, J. Am. Chem. Soc. 78 (1956) 4503–4510.

[18] M.B. Epstein, G.M. Barrow, K.S. Pitzer, F.D. Rossini, Heats, equilibrium constants, and free energies of formation of the dimethylcyclopentanes, J. Res. Natl. Bur. Stand. 43 (1949) (1934) 245–250.

[19] J.E. Kilpatrick, H. Werner, C. Beckett, K.S. Pitzer, F.D. Rossini, Heats, equilibrium constants, and free energies of formation of the alkylcyclopentanes and alkylcyclohexanes, J. Res. Natl. Bur. Stand. 39 (1947) (1934) 523–543.

[20] C.D. Baertsch, K.T. Komala, Y.-H. Chua, E. Iglesia, Genesis of Brønsted acid sites during dehydration of 2-butanol on tungsten oxide catalysts, J. Catal. 205 (2002) 44–57, http://dx.doi.org/10.1006/jcat.2001.3426.

[21] J. Macht, R.T. Carr, E. Iglesia, Consequences of acid strength for isomerization and elimination catalysis on solid acids, J. Am. Chem. Soc. 131 (2009) 6554–6565.

[22] P.B. Weisz, E.W. Swegler, Stepwise reaction on separate catalytic centers: isomerization of saturated hydrocarbons, Science 126 (1957) 31–32, http://dx.doi.org/10.1126/science.126.3262.31 (80-).

[23] F. Alvarez, A. Montes, G. Perot, M. Guisnet, Hydroisomerization and hydrocracking of alkanes: 4. Methylcyclohexane transformation on ptushy catalysts, Stud. Surf. Sci. Catal. 49 (1989) 1367–1376, http://dx.doi.org/10.1016/S0167-2991(08)62021-2.

[24] R.M. Koros, E.J. Nowak, A diagnostic test of the kinetic regime in a packed bed reactor, Chem. Eng. Sci. 22 (1967) 470, http://dx.doi.org/10.1016/0009-2509(67)80134-9.

[25] M. Natal-Santiago, R. Alcalá, J. Dumesic, DFT study of the isomerization of hexyl species involved in the acid-catalyzed conversion of 2-methyl-pentene-2, J. Catal. 181 (1999) 124–144.

[26] W.J. Knaeble, E. Iglesia, unpublished results, (n.d.).

[27] Y.V. Joshi, A. Bhan, K.T. Thomson, DFT-based reaction pathway analysis of hexadiene cyclization via carbenium ion intermediates: mechanistic study of light alkane aromatization catalysis, J. Phys. Chem. B 108 (2004) 971–980, http://dx.doi.org/10.1021/jp036205m.

[28] I.D. Mackie, J. Govindhakannan, G.A. Dilabio, O.P. Drive, C. Tg, Thermochemical and kinetic study of the carbocation ring contraction of cyclohexylium to methylcyclopentylium, J. Phys. Chem. A 112 (2008) 4004–4010, http://dx.doi.org/10.1021/jp710656f.

[29] I.D. Mackie, J. Govindhakannan, Ring contraction mechanisms in substituted cyclohexylium cations, J. Mol. Struct. THEOCHEM. 939 (2010) 53–58, http://dx.doi.org/10.1016/j.theochem.2009.09.040.

[30] V. Vrček, M. Saunders, O. Kronja, Rearrangement pathways of five-membered ring enlargement in carbocations: quantum chemical calculations and deuterium kinetic isotope effects, J. Org. Chem. 68 (2003) 1859–1866, http://dx.doi.org/10.1021/jo020694p.

[31] Y.V. Joshi, K.T. Thomson, Embedded cluster (QM/MM) investigation of C6 diene cyclization in HZSM-5, J. Catal. 230 (2005) 440–463, http://dx.doi.org/10.1016/j.jcat.2004.12.016.

[32] R.a. Alberty, Y.S. Ha, Standard chemical thermodynamic properties of alkylcyclopentane isomer groups, alkylcyclohexane isomer groups, and combined isomer groups, J. Phys. Chem. Ref. Data 14 (1985) 1107, http://dx.doi.org/10.1063/1.555741.

[33] R.a. Alberty, Standard chemical thermodynamic properties of alkylbenzene isomer groups, J. Phys. Chem. Ref. Data 14 (1985) 177, http://dx.doi.org/10.1063/1.555745.

[34] M.B. Epstein, K.S. Pitzer, F.D. Rossini, Heats, equilibrium constants, and free energies of formation of cyclopentene and cyclohexene, J. Res. Natl. Bur. Stand. 42 (1949) (1934) 379, http://dx.doi.org/10.6028/jres.042.031.

[35] M. Peereboom, B. van de Graaf, J.M.A. Baas, Experimental and calculated thermodynamic data for the isomeric methylcyclohexenes and methylenecyclohexane, Recl. Des Trav. Chim. Des Pays-Bas. 101 (1982) 336–338, http://dx.doi.org/10.1002/recl.19821011003.

[36] G.F. Froment, K.B. Bischoff, J. De Wilde, Chemical Reactor Analysis and Design, third ed., Wiley, Hoboken, NJ, 2010.

[37] R. Aris, On shape factors for irregular particles—I, Chem. Eng. Sci. 6 (1957) 262–268, http://dx.doi.org/10.1016/0009-2509(57)85028-3.

[38] J.A. Martens, P.A. Jacobs, Introduction to Zeolite Science and Practice, Elsevier, 2001, http://dx.doi.org/10.1016/S0167-2991(01)80256-1.

[39] J.M. Zalc, S.C. Reyes, E. Iglesia, The effects of diffusion mechanism and void structure on transport rates and tortuosity factors in complex porous structures, Chem. Eng. Sci. 59 (2004) 2947–2960, http://dx.doi.org/10.1016/j.ces.2004.04.028.

[40] S.C. Reyes, E. Iglesia, Effective diffusivities in catalyst pellets: new model porous structures and transport simulation techniques, J. Catal. 129 (1991) 457–472, http://dx.doi.org/10.1016/0021-9517(91)90049-A.

[41] M.T. Aronson, R.J. Gorte, W.E. Farneth, The influence of oxonium ion and carbenium ion stabilities on the Alcohol/H-ZSM-5 interaction, J. Catal. 98 (1986) 434–443, http://dx.doi.org/10.1016/0021-9517(86)90331-3.

[42] A. Corma, Inorganic solid acids and their use in acid-catalyzed hydrocarbon reactions, Chem. Rev. 95 (1995) 559–614.

[43] W.E. Farneth, R.J. Gorte, Methods for characterizing zeolite acidity, Chem. Rev. 95 (1995) 615–635, http://dx.doi.org/10.1021/cr00035a007.

[44] R.J. Gorte, What do we know about the acidity of solid acids?, Catal Letters 62 (1999) 1–13.

[45] P. Deshlahra, R.T. Carr, E. Iglesia, Ionic and covalent stabilization of intermediates and transition states in catalysis by solid acids, J. Am. Chem. Soc. 136 (2014) 15229–15247, http://dx.doi.org/10.1021/ja506149c.